2010

Anterior-posterior impedance cardiography: a new approach to accurate, non-invasive monitoring of cardiac function

Charles F. Babbs
Purdue University, babbs@purdue.edu

Anterior-posterior impedance cardiography: a new approach to accurate, non-invasive monitoring of cardiac function

Charles F. Babbs, MD, PhD

Weldon School of Biomedical Engineering, Purdue University, West Lafayette Indiana

Abstract

The conventional impedance cardiogram is a record of pulsatile changes in the electrical impedance of the chest with each heartbeat. The signal seems intuitively related to cardiac stroke volume. However doubts persist about the validity of stroke volume measurements based on electrical impedance. This paper presents a new electrical axis for impedance cardiography that is perpendicular to the conventional head-to-foot axis in an anterior-posterior direction. Dual chest and back electrodes are concentric, permitting tetrapolar technique. A relatively simple analytical model is developed, and this model is validated in a three-dimensional finite element model of current flow through the human chest. Three-dimensional simulations show predictable relationships between the fractional increase in anterior-posterior chest impedance and the ventricular ejection fraction (cardiac stroke volume / ventricular end-diastolic volume). Ejection fraction can be computed accurately with a roughly 30-fold increase in signal level compared to the conventional impedance cardiogram. Breathing causes only modest changes in the signal. When the axis of current flow is optimized, one can interpret the impedance changes during the cardiac cycle with greater confidence as a painless, noninvasive, beat-by-beat indicators of ventricular ejection fraction in a wide variety of clinical settings.

Key words: blood flow; cardiac output; ejection fraction, hemodynamic monitoring, stroke volume

Introduction

Creation of a satisfactory method to measure cardiac function non-invasively on a beat-by-beat basis has remained an open problem in biomedical engineering. Impedance cardiography, first described by Nyboer in 1940[1, 2] and later applied to monitoring of astronauts[3] has provided an approximate solution. The conventional impedance cardiogram is a record of variations of chest impedance, obtained using painless, high frequency, non-stimulating, electric current passed in the head-to-foot axis from the base of the neck to the upper abdomen (Figure 1). The frequency of the current passing through the chest and heart is high enough to prevent sensation or muscle stimulation but low enough so that the pattern of current flow is similar to that of direct current. Strictly speaking, impedance is the opposition to flow of sinusoidal electric current, whereas resistance is the opposition to flow of steady, direct current. Tissue impedance at 100,000 cycles/sec (100 kHz) is about 15 percent less than ordinary electrical resistance[4]. However, at the frequencies required for impedance cardiography, one can think of the macroscopic pattern of current flow through the body as being similar to that of direct current.

The instantaneous tracing of chest impedance as a function of time fluctuates in a characteristic way during each cardiac cycle. Traditionally chest impedance is recorded between the thoracic inlet at the base of the neck and the thoracic outlet at the level of the diaphragm (Figure 1). Unlike the electrocardiogram, which provides direct information only about the pattern of electrical activation and recovery of the heart—not about dynamics—the impedance signal is obviously related to changes in the size and composition of blood containing structures within the chest. In this sense the impedance cardiogram promises to reveal meaningful information about effectiveness of the heart as a pump on a beat-by-beat basis, potentially useful for monitoring of critically ill patients and patients undergoing anesthesia, especially in cases where blood volume or cardiac output may change significantly.

The early laboratory studies of Kubicek in anesthetized dogs[3] suggested that the impedance cardiogram provides a measure of left ventricular function, but the exact mechanism generating the fall in impedance during ventricular ejection has remained elusive. Although indices derived from the chest impedance signal track cardiac stroke volume very well[4-6], the absolute values of stroke volume in units of milliliters of blood per heartbeat have been considered unreliable and suspect[7-10], especially in the case of congestive heart failure, when ventricular ejection fraction is greatly diminished[8, 11, 12], or in patients with either reduced or increased peripheral vascular resistance[13]. In addition, comparisons of impedance based stroke volume and cardiac output with results from the green dye dilution or the Fick methods show that the impedance cardiogram tends to overestimate stroke volume by 5 to 10 percent, with rather wide standard deviations, leading to the conclusion that the impedance method is not accurate[4]. Recent studies have emphasized that changes in impedance of lungs, great vessels, cardiac atria, and cardiac ventricles, during the cardiac cycle are complex and countervailing, leading to a small net signal of uncertain origin[9, 13]. In sick patients with varying pathophysiology,

such as reduced ventricular ejection fraction or reduced peripheral vascular, the factors that combine to give reasonable predictions in more healthy individuals may fail. Accordingly, interpretations of impedance cardiographic data have tended to be tentative and guarded, and acceptance of the technique is not widespread[5, 8].

Such impediments to progress can be removed by looking at impedance cardiography from a new perspective—front to back, rather than neck to abdomen—and considering an electrode arrangement that forces current substantially through the cardiac ventricles. The objective of the present paper is to explore this alternative anatomic axis for impedance cardiography. Anatomic and physiologic modeling of this fresh approach lead to several surprising results, and to the real possibility that impedance based methods can provide accurate painless noninvasive cardiac monitoring on a beat-by-beat basis.
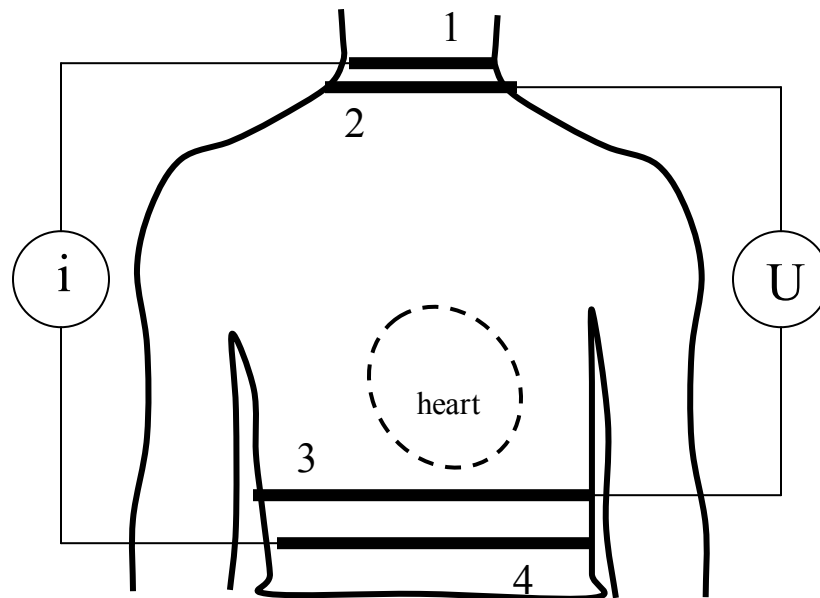

Figure 1. Four-electrode system for recording a conventional impedance cardiogram. Flexible, band-like electrodes 1, 2, 3, and 4 are shown. A constant intensity, high frequency, non-stimulating sinusoidal current, i, is passed between outer electrodes 1 and 4. The resulting voltage, U , is measured between inner electrodes 2 and 3. This is called tetrapolar technique.

Theory

Measurement of conventional chest impedance along the head-to-foot axis

Figure 1 illustrates the placement of electrodes used to record the conventional impedance cardiogram. To measure the impedance of the whole chest cavity, a low-level, constant sinusoidal current (~ 3 mA at 100 kHz) is injected through the chest from soft ring electrodes, labeled 1 and 4, made of electrically conductive tape, placed around the neck and abdomen. The resulting demodulated root mean square potential, U, is measured between a pair of similar inner electrodes, labeled 2 and 3, at the top and bottom of the chest cavity proper. (This is known as tetrapolar – or 4 electrode – technique[11].) If the impedance, Z, of the chest increases, then U will increase, because current is constant and voltage is the product of current and impedance (U = i Z). This tetrapolar technique provides much more stable and reliable signals than the original two-electrode technique, particularly those due to respiration, which occur as a result of contact resistance changes in a bipolar systems[11].

If a generalized column of tissue such as the thorax with essentially parallel sides has overall electrical resistance R, length L, cross sectional area A, and resistivity ρ, then the classical electrical resistance is

$$R = \rho \frac{L}{A}.$$ (1)

This equation[4] can describe the effects of macroscopic tissue geometry in terms of the effective length and cross section of the chest, L and A. The resistivity of blood is about 150 ohm-cm, and that of heart muscle is about 300 ohm-cm[4]. The resistivity of lung is about 1500 ohm-cm[4]. In impedance cardiography the magnitude of the impedance, Z, at 100 kHz, expressed in units of ohms, is somewhat less that resistance, R, by a proportional constant that depends on the properties of the tissue and the frequency of the current[14]. However, if changes in impedance with heart function are interpreted in terms of the relative changes in impedance during the cardiac cycle, the proportional constant can be ignored, and one can create conceptual models based on the direct current analogs.

Because the resistivity of blood is less than that of heart muscle and much less than that of lung, theorists have sought to explain the impedance cardiogram on the basis of changing blood volume within the chest as the heart beats. A working hypothesis as to the genesis of the impedance cardiogram[3, 9] is that ejection of blood from the left ventricle into the thoracic aorta causes a net decrease in overall chest impedance. The positive impedance change caused by the blood volume reduction in the heart chambers is balanced by the negative impedance changes caused by the expansion of blood vessels in the lungs and expansion of the thoracic aorta as they receive blood from the cardiac ventricles during ejection. These increases and decreases in impedances of intrathoracic structures largely cancel under normal physiological conditions[9], as blood is moved

mostly from one part of the chest to another. Such complex patterns of blood flow have resisted theoretical interpretation[9, 12, 15].

Proposed measurement of chest impedance along a front-to back axis

As the cardiac ventricles squeeze blood into the aorta and the pulmonary artery during ejection, they develop both a larger length to area ratio (L/A) and also a larger composite resistivity, as low resistivity blood is squeezed out. The effective resistance of the ventricles, modeled either as in Equation (1) or in a more anatomically realistic way[9], is clearly increased as blood is ejected during cardiac systole. The present paper is dedicated to the proposition that the local impedance change derived predominantly from the cardiac ventricles may provide a better representation of heart function than the conventional impedance cardiogram. The key idea is to change the electrode arrangement by which the impedance is recorded, as shown in Figure 2, so as to reduce current through the lungs, aorta, and vena cavae and to increase current through the cardiac ventricles. Current is more selectively passed through the ventricles from front to back, avoiding most of the thoracic aorta, lungs, and vena cavae with their attendant decreases in impedance during ventricular ejection.
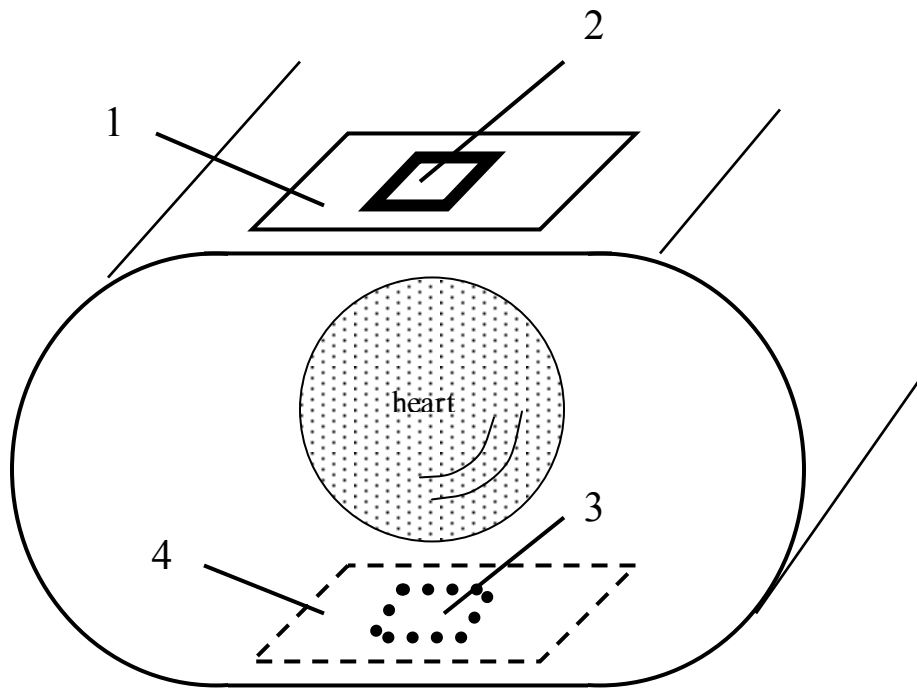

Figure 2. Tetrapolar rectangular ring and spot electrodes for impedance recording. The twin front and back electrodes are centered over the cardiac ventricles to maximize the signal produced by ventricular emptying and minimize signals associated with expansion of the aorta, vena cavae, and larger pulmonary arteries.

Figure 2 illustrates a tetrapolar front-to-back electrode arrangement for recording changes in heart impedance. The front or anterior electrodes 1 and 2 are centered over the cardiac notch in the left lung, slightly left of midline. This position focuses current on the cardiac ventricles. The back electrodes 3 and 4 are located on the skin of the back immediately opposite the front electrodes. A tetrapolar recording arrangement is achieved by a concentric ring electrode design with voltage sensing spot electrodes 2 and 3 in the centers of the each front and back pair. These inner voltage-sensing electrodes are surrounded by concentric insulating spaces and then the outer current injecting electrodes 1 and 4. This electrode geometry permits the stability and accuracy of a tetrapolar impedance recording system[4].

A simple analytical model

In order to relate the change in impedance to heart pumping action, it is helpful to develop an analytical model that describes how inter-electrode impedance changes as blood is squeezed out of the heart. One approach to such an analytical model (there are many possibilities) is as follows.

Three parallel paths: heart, lungs, and abdomen

If the current injecting electrodes 1 and 4 are sufficiently large and of equal area, the current flow from front to back becomes roughly parallel. In this case analytical variants of Equation (1) can be applied. The front to back current can be regarded as taking one of three routes, as shown in Figure 3. Route 1 is a column of tissue passing though the heart itself, including cardiac muscle, intracavitary blood, part of the thoracic spine, and some surrounding lung. The boundary of this cardiac column, here denoted Column 1, is always considered to be located at the outer boundary of cardiac muscle. As the heart contracts in systole, this central cardiac column becomes narrower, and the composition of tissue therein changes as blood is ejected from the ventricles. During ejection blood volume is swapped for lung tissue within this column. The volume of cardiac muscle, by definition, is constant within the column, and bone, by definition is immobile.

The second column of tissue, denoted Column 2, is composed of lung tissue and chest wall that lies between the electrodes but not in line with the heart. Column 2 also includes fringing lung tissue intercepted by spreading current lines at the outer edges of electrodes 1 and 4. As the heart contracts the inner border of this hollow column expands slightly to fill some of the space vacated by contracting ventricular muscle.

The third column of tissue (not shown in Figure 3(b)) includes the fringing field of current that passes not through lung, but through the upper abdomen and diaphragm. This shunt resistance is anatomically necessary, because the heart rests on the diaphragm. The resistivity of the soft tissues of the upper abdomen is greater than that of blood (especially if a gastric gas bubble and gas bubbles in the transverse colon are present), but much less than that of lung. These tissues below the diaphragm constitute Column 3.
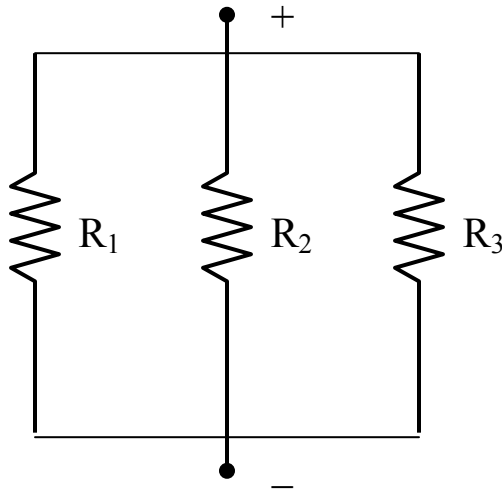
Figure 3(a) Equivalent circuit for chest impedance recording with front to back electrodes. R_1 represents impedance of the lower third of the mediastinum, including the heart. R_2 represents impedance of the lower third of lung fields between current injecting electrodes. R_3 represents impedance of the shunt path through upper abdomen.
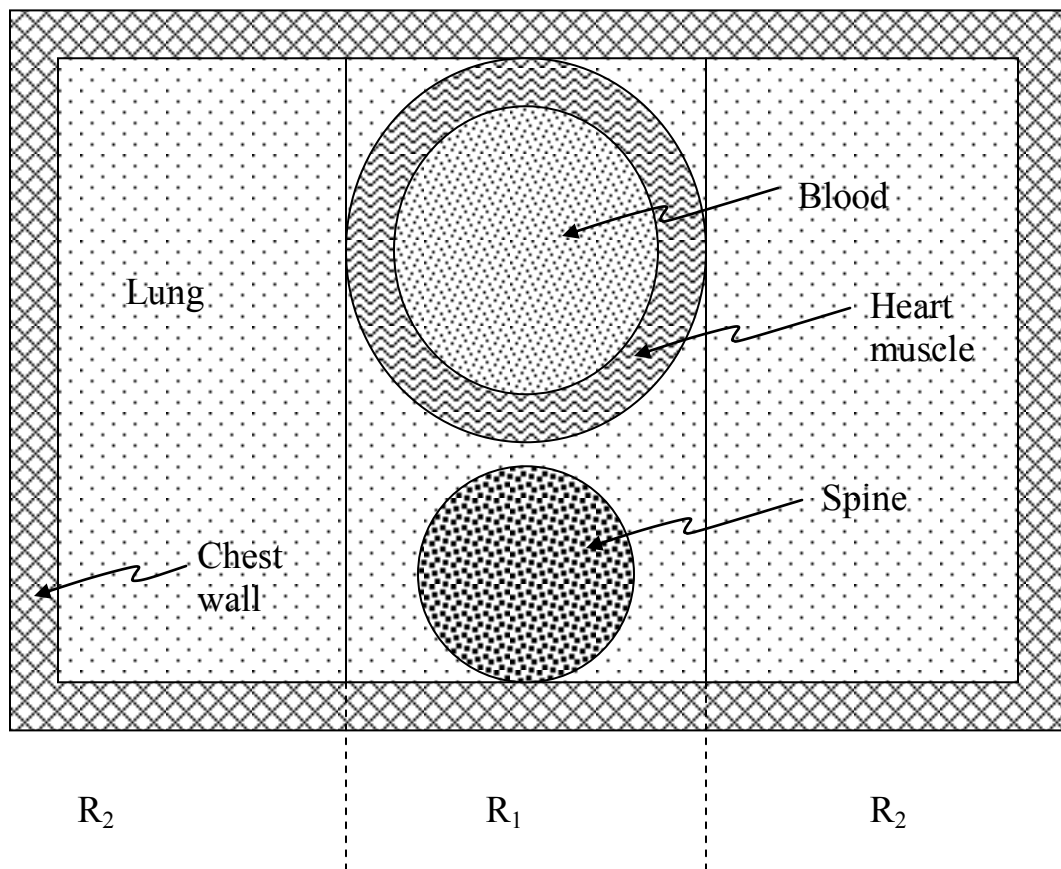
Figure 3(b) chest components of equivalent circuit R_1 in parallel with R_2.

$$R = \frac{\rho L}{A}$$

$$\rho = \sigma_1 \rho_1 + \sigma_2 \rho_2 + \sigma_3 \rho_3 + \cdots$$

Figure 4(a). Model for resistivity of composite material of path R_1 with parallel current flow.

Figure 4(b) Vertical layering effect of component tissues in the lower third of the mediastinum.

Column 1 as a composite material

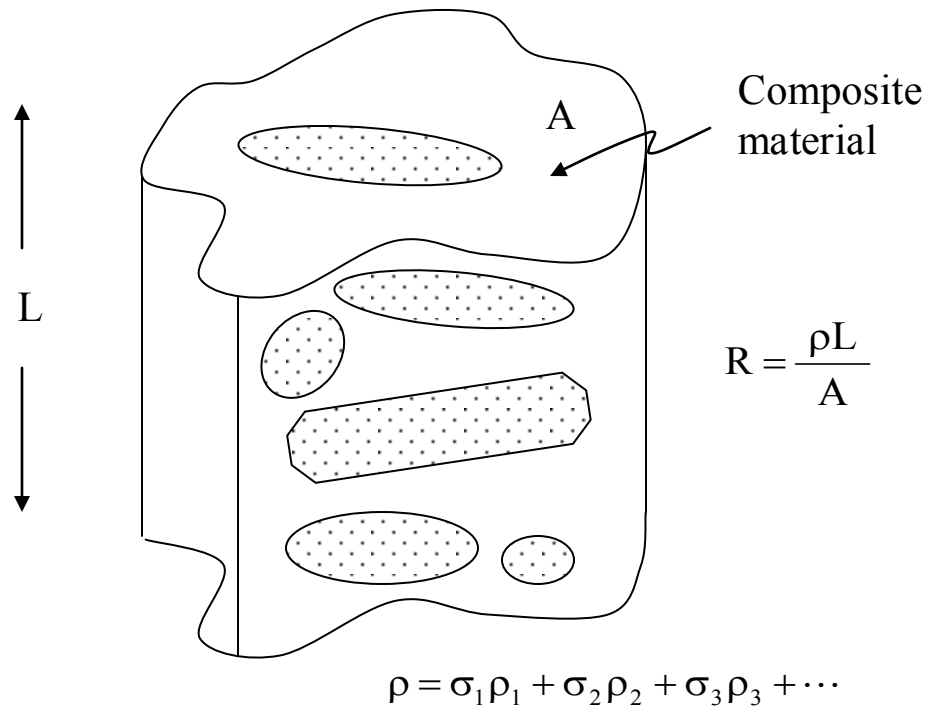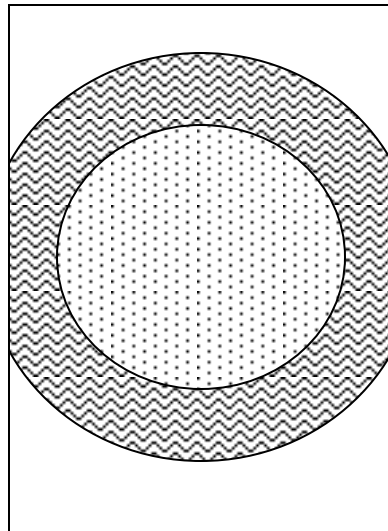Consider first the changes in Column 1 during ventricular ejection. The basal state is that existing at end-diastole, just before ventricular ejection begins. Consider the aggregate resistivity of this tissue mix as a linear combination by volume of the resistivities of blood, muscle, bone, and lung within Column 1 (Figure 4(a)). Here a composite resistivity model, as opposed to a composite conductivity model, is appropriate, since the various materials tend to be layered perpendicular to current flow, as indicated in Figure 4(b) (skin, bone, lung, muscle, blood, muscle, bone, skin).

The composite resistivity of the Column 1 is thus a volume-weighted linear combination

$$\rho_1 = \sigma_b \rho_b + \sigma_L \rho_L + \sigma_m \rho_m + \sigma_s \rho_s, \qquad\qquad (2)$$

where end-diastolic volume fractions σ of blood, lung, cardiac muscle, and spine within Column 1 are denoted by subscripts b, L, m, and s, and similarly for specific tissue resistivities, ρ.

Let x indicate the fraction of total stroke volume ejected from either the right or left ventricles during cardiac contraction. This variable is well known in cardiology as the ejection fraction, sometimes abbreviated EF[*]. The resistance of Column 1 as a function of x is

$$R_1(x) = \frac{\rho_1(x)\,L}{A_1(x)}. \qquad\qquad (3)$$

Let us first deal with the changes in composite resistivity, $\rho_1(x)$. As blood exits Column 1 during ejection it is replaced with compliant lung tissue. By definition all of the cardiac muscle is included in Column 1, and the volume fraction of bone is essentially constant. As blood is swapped for lung during ejection, we have

$$\sigma_b(x) = \sigma_b(0)(1-x) \quad \text{and} \quad \sigma_L(x) = \sigma_L(0) + x\sigma_b(0). \qquad\qquad (4)$$

---

[*] The change in heart volume is the integral of the difference between empting rate and filling rate of the heart during systole. If only the cardiac ventricles are within the volume sampled by impedance recording then the measured ejection fraction is the same as the true ventricular ejection fraction. If the cardiac atria are also sampled and we assume temporarily that the rate of venous return is nearly constant, then the amount of atrial filling during ventricular systole is the same as the mean flow, multiplied by the ejection time. In this case the sensed or effective ejection fraction is diminished by a factor of $(1 - t_e/T)$, where t_e = systolic ejection time, T = cycle time (1/cardiac frequency). In the remaining discussion ejection fraction and stroke volume are taken to mean the effective or net ejection fraction, including any sensed venous return to the atria. In a future computer based system times t_e and T could be, if needed, obtained by waveform analysis of the front-to-back impedance cardiogram itself.

Combining (2) and (4), the composite resistivity in Column 1 is

$$\rho_1(x) = \rho_1(0)\left(1 + \frac{\rho_L - \rho_b}{\rho_1(0)}\sigma_b(0)x\right). \tag{5a}$$

A remaining complexity is the dependence of lung resistivity, ρ_L , on the net ejection fraction, x. The volume fraction of blood in the lungs changes as blood is ejected into the pulmonary arteries and drains gradually from the pulmonary veins into the left atrium. Hence the resistivity of lung tissue decreases during ventricular systole[9]. As shown in Appendix 1, this effect can be accounted by the simple correction

$$\rho_L(x) = \frac{\rho_L(0)}{1 + \beta_L x} \approx \rho_L(0)(1 - \beta_L x), \tag{5b}$$

where for right ventricular end diastolic volume, $V_{RV}(0)$, and lung volume V_L, the small constant

$$\beta_L = \frac{\rho_L(0)}{\rho_b}\frac{V_{RV}(0)}{V_L}.$$

Now, the composite resistivity of Column 1 as an explicit function of net ejection fraction is

$$\rho_1(x) = \rho_1(0)\left(1 + \frac{\rho_L(0) - \rho_b}{\rho_1(0)}\sigma_b(0)x - \beta_L\frac{\rho_L(0)}{\rho_1(0)}\sigma_b(0)x^2\right). \tag{5c}$$

Next, let us deal with the cross sectional area, $A_1(x)$. Area A_1 is defined as the area shadowed by the heart. Total heart volume $V_h = V_b + V_m$, includes both blood and cardiac muscle. In turn, $V_h = A_1 L(\sigma_b + \sigma_m)$. So, for ejection fraction $x = 1 - V_b(x)/V_b(0)$, we can write

$$A_1(x) = \frac{V_h(x)}{L(\sigma_b + \sigma_m)} = \frac{V_h(0) - V_b(0)x}{L(\sigma_b + \sigma_m)} = A_1(0)\left(1 - \frac{V_b(0)}{V_h(0)}x\right) = A_1(0)(1 - \phi x), \tag{6}$$

where $\phi = \frac{\sigma_b(0)}{\sigma_b(0) + \sigma_m(0)}$, a parameter describing the degree of diastolic filling of the heart with blood prior to ejection. A normal value for ϕ is about 0.5.

Combining results (5) and (6) for composite resistivity and for area, we have

$$R_1(x) = \frac{\rho_1(x)L}{A_1(x)} = \cdot \frac{\rho_1(0)\left(1 + \frac{\rho_L - \rho_b}{\rho_1(0)}\sigma_{bl}x - \beta_L\frac{\rho_L(0)}{\rho_1(0)}\sigma_b(0)x^2\right)L}{A_1(0)(1 - \phi x)}$$

or

$$R_1(x) = R_1(0)\frac{\left(1 + \frac{\rho_L - \rho_b}{\rho_1(0)}\sigma_b x - \beta_L\frac{\rho_L(0)}{\rho_1(0)}\sigma_b(0)x^2\right)}{(1 - \phi x)}. \tag{7}$$

Thus the change of resistance of Column 1 is a defined function of ejection fraction, x, and constants that describe the anatomy and electrical resistivity of chest tissues.

Volume compensation in Column 2

In addition to these major changes in Column 1 there are also smaller changes in Column 2, which expands inwardly during heart contraction. Assuming that the change in lung resistivity during ejection is given by (5b),

$$R_2(x) = \frac{\rho_L(x)L}{A_2(0) + A_1(0)\phi x} = \frac{\rho_L(0)L}{A_2(0)\left(1 + \frac{A_1(0)}{A_2(0)}\phi x\right)(1 + \beta_L x)}, \tag{8a}$$

or

$$R_2(x) = \frac{R_2(0)}{1 + \left(\frac{A_1(0)}{A_2(0)}\phi + \beta_L\right)x + \frac{A_1(0)}{A_2(0)}\phi\beta_L x^2}. \tag{8b}$$

As ejection fraction, x, increases, the resistance R_1 of the cardiac column increases and resistance R_2 of the lungs decreases slightly. The resistance of the abdominal shunt path, R_3, is considered constant.

Resistance changes in parallel paths 1, 2, and 3 with ejection

The total combined resistance, R, for parallel paths R_1, R_2, and R_3 comes from the standard expression for parallel resistors, $1/R = 1/R_1 + 1/R_2 + 1/R_3$.

Combining expressions (7) and (8) for R_1, R_2, and R_3 in this way,

$$\frac{1}{R(x)} = \frac{1}{R_1(0)}\frac{(1-\phi x)}{(1+\alpha_1 x - \alpha_2 x^2)} + \frac{1}{R_2(0)}(1+\alpha_3 x + \alpha_4 x^2) + \frac{1}{R_3(0)},$$ (9a)

where constants

$$\alpha_1 = \frac{(\rho_{lu} - \rho_{bl})\sigma_{bl}}{\rho_1(0)}, \quad \alpha_2 = \frac{\beta_L \rho_{lu}(0)\sigma_{bl}}{\rho_1}, \quad \alpha_3 = \frac{A_1(0)}{A_2(0)}\phi, \text{ and } \alpha_4 = \frac{A_1(0)}{A_2(0)}\phi\beta_L.$$ (9b)

The post/pre ejection resistance ratio, as a function of ejection fraction, x,

$$\frac{R(x)}{R(0)} = \frac{1}{\frac{R(0)}{R_1(0)} \cdot \frac{1-\phi x}{1+\alpha_1 x - \alpha_2 x^2} + \frac{R(0)}{R_2(0)} \cdot (1+\alpha_3 x + \alpha_4 x^2) + \frac{R(0)}{R_3(0)}},$$ (10a)

or

$$\frac{R(x)}{R(0)} = \frac{1+\alpha_1 x - \alpha_2 x^2}{\lambda_1(1-\phi x) + \lambda_2(1+\alpha_3 x + \alpha_4 x^2)(1+\alpha_1 x - \alpha_2 x^2) + \lambda_3(1+\alpha_1 x - \alpha_2 x^2)}$$ (10b)

for $\lambda_1 = \frac{R(0)}{R_1(0)}$, $\lambda_2 = \frac{R(0)}{R_2(0)}$, $\lambda_3 = \frac{R(0)}{R_3(0)}$, and $\lambda_1 + \lambda_2 + \lambda_3 = 1$.

Let $y(x)$ represent relative change in chest impedance caused by a given ejection fraction: $y(x) = R(x) / R(0)$. Then, neglecting terms of order x^3 or higher, which are small,

$$y = \frac{1 + k_1 x - k_2 x^2}{1 + k_3 x + k_4 x^2}$$ (10c)

for hybrid constants k_1 through k_4, which depend on anatomically defined system parameters that describe the pre-ejection state, with

$$k_1 = \alpha_1$$
$$k_2 = \alpha_2$$
$$k_3 = (\alpha_1 + \alpha_3)\lambda_2 + \alpha_1 \lambda_3 - \phi\lambda_1 \quad .$$
$$k_4 = \alpha_1 \alpha_3 \lambda_2 - \alpha_2 \lambda_3 + \alpha_4 \lambda_2$$

This quadratic equation in ejection fraction, x, has value 1.0 at $x = 0$ and increases in a slightly decelerated fashion by virtue of the $-k_2x^2$ term and the terms in the denominator. For typical normal values we have $k_1 \sim 0.3$, $k_2 \sim 0.05$, $k_3 \sim 0.1$, and $k_4 \sim 0.03$. Thus the denominator of (10c) is close to 1. As is evident from the definition of $k_1 = \alpha_1$ in (9b), constant k_1 describes the difference between lung and blood resistivity and amount of blood in the heart, which conspire to cause resistance to increase as blood is ejected from the ventricles. Constant $k_2 = \alpha_2$ in (9b) describes the decrease in lung resistivity caused by ejection of low resistivity blood into the lungs during ventricular systole. Constants k_3 and k_4 describe increased current shunting around the heart as the ventricles contract.

One can get an intuitive feel for the form function (10c) as follows. For small values ε << 1 the binomial series approximation $1/(1+\varepsilon) \approx 1-\varepsilon$, so for smaller net ejection fractions, x, we would have $y \approx 1 + (k_1 - k_3)x$. This means that the fractional or percentage increase in resistance $y-1$ is roughly proportional to ejection fraction, x. For larger ejection fractions the influence of the smaller remaining terms in (10c) causes a roll off in the resistance increase as a function of ejection fraction.

This quadratic equation (10c) can be rearranged in familiar form to allow for straightforward solution for net ejection fraction, x, given the measured systolic/diastolic resistance or voltage ratio, y, as

$$(k_4y + k_2)x^2 + (k_3y - k_1)x + y - 1 = 0 . \tag{11}$$

Some model parameters will, of course, change during breathing. These include the dimensions of the chest, the resistivity of the lungs, and the shunt resistance, R_3, which will each increase to modulate the observed impedance change with each heartbeat. A detailed simulation of the effect of breathing is shown in the Results section.

Between breaths the hybrid model parameters k_1 through k_4 are well behaved, and for the most part easily measured or estimated. Anatomic constants such as the volume fractions of blood, cardiac muscle, and lung in the lower third of the mediastinum can be estimated for normal humans by analysis of CT scans of the chest. They are not time varying, since only the end-diastolic values are needed. We expect the volume fractions to be similar for large and small adults. As long as the electrode areas are larger than the cross section of the ventricles, the model parameters are not sensitive to small changes in the position of the heart between the front and back electrodes. The normal values can be modified to represent different pathologies such as congestive heart failure or hypovolemic shock. Virtual handbooks could be created to match constants to particular patients according to diagnosis. Thus the analytical model provides a route for determining ventricular ejection fraction from measured impedance changes using anterior to posterior ring electrodes.

In particular the ejection fraction can be calculated from the post/pre ejection voltage ratios, y, recorded from the tetrapolar electrode system by solving quadratic equation (10c) for ejection fraction x, given the observed post/pre ejection impedance ratio, y.

Validation in a computational model

One way to test the reasonableness of the forgoing analytical model of Equations (10a) through (10c) using a biomedical engineering approach is to compute chest impedance changes in a three-dimensional model of the human torso composed of finite elements. In this way one can explore complex current distributions and the way body surface potentials reflect underlying tissue impedance changes in three dimensions.

It is easy to create a satisfactorily realistic finite element model of the chest in three dimensions using multiple overlapping spherical primitives, each with a defined center, radius, and resistivity. In a standard, reference model, for example, the volume of the torso is approximated by a rectangular volume of length 50 cm, width 30 cm, and depth 20 cm. Space outside the model has air resistivity ($\sim 10^{12}$ ohm-cm). The spine is modeled as a chain of partially overlapping spheres of bone resistivity, which resemble the vertebrae. Similarly, soft issues of the mediastinum, including the esophagus and great vessels are measured as chains of closely overlapping spheres. For each successive spherical primitive, p, the resistivity of any control volume lying within the radius of p is set to the resistivity of p, overwriting any previous values.

In this way complex structures can be sculpted in the workspace as if painting with a broad brush in three dimensions. Erasing or eroding can be done by over-painting with a background resistivity. The order of placement of primitives becomes important for the final composition. In the problem at hand the cardiac ventricles are represented by spheres of cardiac muscle overwritten by a smaller sphere of blood to make a concentric muscle-blood composite, representing the combined right and left ventricles. (Here with interventricular septum omitted for simplicity.) To model ejection of blood from the ventricles, the radius of the blood volume is diminished to obtain a chosen stroke volume, and the muscle volume radius is diminished so as to maintain a constant volume of cardiac muscle.

One can sculpt an adequate model from simple spherical and rectangular primitives to test for proof of concept. Walls of the rectangular chest cavity, 1 cm thick, are given a composite resistivity of 500 ohm-cm representing skeletal muscle and bone. The chest cavity is filled initially with lung resistivity (1500 ohm-cm) material, which is selectively replaced with overlapping spheres representing the vertebral chain (3000 ohm-cm), mediastinal soft tissues (300 ohm-cm), and the spherical model of the heart (300 ohm-cm for cardiac muscle, 150 ohm-cm for blood). A dome of abdominal soft tissue (300 ohm-cm) is added below the heart to represent the diaphragm and sub-phrenic organs.

Viewing anatomical models in three dimensions

As an aid to sculpting anatomically realistic finite element models, one can create two-dimensional projections of the average resistivity along each straight-line path through the model parallel either to the front-to-back or to the right-to-left axis. The resulting

images are much like clinical X-ray films showing shadows of the simulated organs in place. A pair of orthogonal projections gives good understanding of spatial localization of structures, just as a posterior-anterior and lateral chest films do in routine medical practice. Sample models showing thorax, heart, lungs, diaphragm, abdominal organs, spine, and the soft tissues of the mediastinum are illustrated in Table 1 and Figure 5.

Table 1. Properties of spherical primitives for a simple 3D chest model.

| Resistivity (ohm-cm)	Center x (cm)	Center y (cm)	Center z (cm)	Radius (cm)	Anatomical description
1500	15	25	10	100	lung tissue (default)
300	15	60	10	31	abdomen soft tissues
3000	15	5	17	3	spine
3000	15	10	17	3	spine
3000	15	15	17	3	spine
3000	15	20	17	3	spine
3000	15	25	17	3	spine
3000	15	30	17	3	spine
3000	15	35	17	3	spine
3000	15	40	17	3	spine
3000	15	45	17	3	spine
3000	15	50	17	3	spine
300	15	2.5	8	4	soft tissue of mediastinum
300	15	5	8	4	soft tissue of mediastinum
300	15	7.5	8	4	soft tissue of mediastinum
300	15	10	8	4	soft tissue of mediastinum
300	15	12.5	8	4	soft tissue of mediastinum
300	15	15	8	4	soft tissue of mediastinum
300	15	17.5	8	4	soft tissue of mediastinum
300	16.5	20	8	4	soft tissue of atria
300	18	25	7.5	6	heart muscle
150	18	25	7.5	5	heart blood
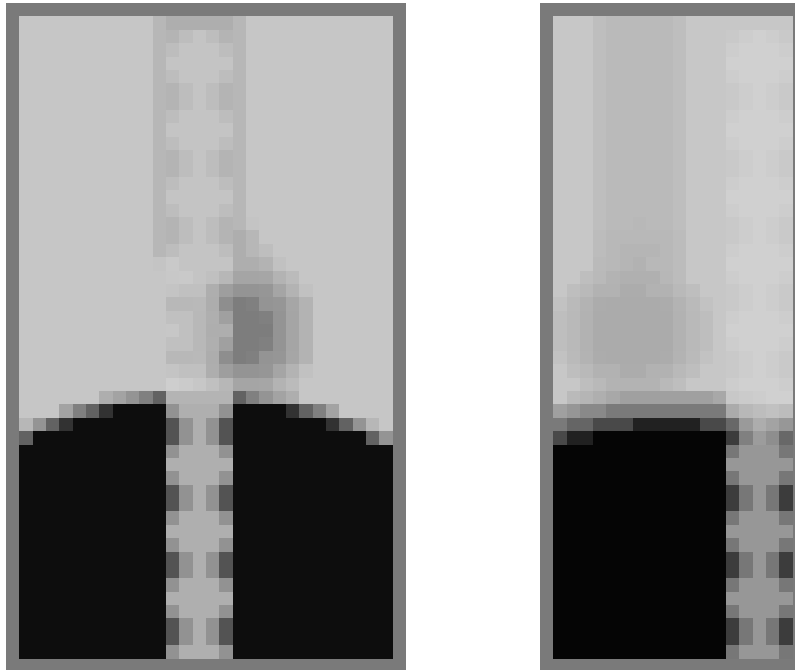
Figure 5. Quasi-radiographic images of the chest model. Darker areas represent greater average conductivity, and lighter areas represent greater average resistivity in the posterior-anterior projection (left) and the lateral projection (right).

Numerical methods

A three dimensional workspace of cubical finite elements in a 6-way mesh was created using a personal computer. Front and back electrode potentials were set to constant initial values, and the steady state voltages at the centers of each control volume in the finite element model were determined by iterative solutions of node potentials so as to satisfy Kirchoff's current law for each node. Iteration was continued until the root mean square potential difference between successive iterations for the entire model diminished to less than one part in 10^8 of the potential difference across electrodes 1 and 4. Further details of the numerical methods are provided in Appendix 2.

A two-stage simulation revealed effects of ventricular contraction producing an exactly known ejection fraction in the presence of a constant current source. A model representing end-diastole was solved first. The total current passing through the electrodes was computed using Ohm's law, and the electrical potentials at each node in the 3D workspace were corrected to represent a constant current of 1 mA. In this way a "constant current source" was simulated. Next the dimensions of he heart were updated to reflect ventricular contraction for a specified ejection fraction and the model was re-run to find equilibrium potentials. Again the total current was computed and the voltages adjusted to reflect a total current of 1 mA.

The distribution of potentials on the front (anterior) chest surface was saved for both pre and post ejection simulations and the voltage step-up on the anterior chest at each surface node was computed $(U_{post} - U_{pre}) / U_{pre}$. This relative voltage step-up represents the signal for a constant current, tetrapolar electrode system. In particular, the maximum voltage step-up on the anterior chest, which would be recorded by electrode 2 of the anterior ring electrode system in Figure 2 (the back electrode potential being defined as zero), constitutes the simulated output signal for a tetrapolar system and was interpreted as y in expression (10c). As an aid to visualization of the current density distribution, the scalar amplitude of the current vector at each node in x, y, z space was calculated. The anterior-posterior and lateral projections of average current for the whole model were displayed quasi-radiographically, as just described for resistivity projections.

Results

Figure 6 shows projections of current density through the 3D model for 11 x 21 cm^2 front to back electrodes, centered over the simulated heart. Figure 6(a) shows the pre-ejection current density pattern. Figure 6(b) shows the end-ejection current density pattern for an ejection fraction of 95 percent (an extreme case). Current is funneled from front to back through the heart, which forms a low resistivity pocket within the background matrix of high resistivity lung. With contraction of the heart the current path becomes narrower.
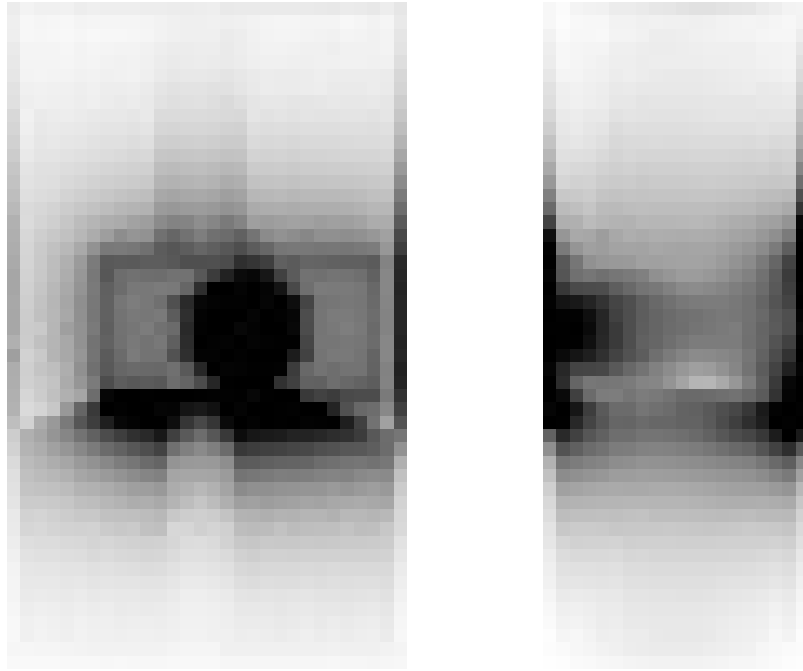
Figure 6(a). End diastolic current density patterns in AP (left) and lateral (right) projections.
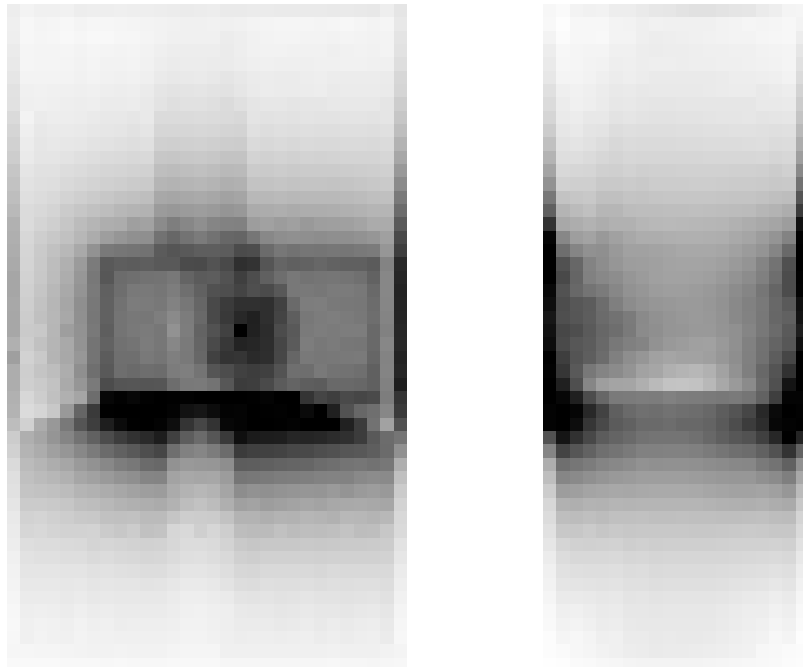

Figure 6(b). Post-ejection current density patterns in AP (left) and lateral (right) projections.

Figure 7 illustrates a map of the fractional increases in anterior chest wall potentials for the constant current source as a result of heart contraction and ventricular ejection. Here the plane of the posterior chest wall is defined as zero potential. In this simulation blood returning to the cardiac atria and vena cavae during the brief ejection period was not modeled, and would be expected to diminish the ventricular signal by about 10 percent.
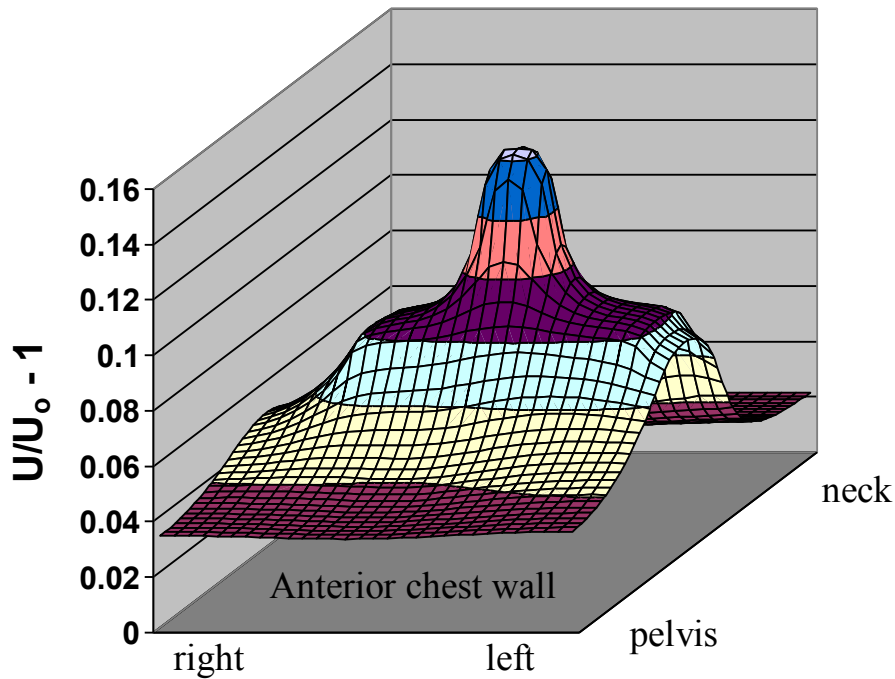

Figure 7. Relative change in anterior chest surface potential, U, caused by ejection of 95 percent of blood from a spherical heart in a three-dimensional finite element model of the human chest. U represents post-ejection electrical potential on the chest surface. U_0 represents the pre-ejection potential.
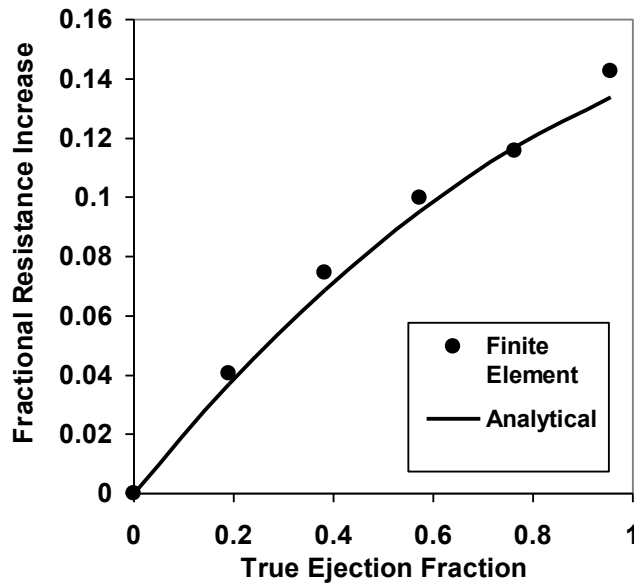
Figure 8. Relative change in chest impedance recorded with the concentric tetrapolar electrodes of Figure 2 for various ventricular ejection fractions using the model of Table 1. Data points represent results for a three-dimensional finite element model. The smooth curve represents a corresponding analytical model based on expressions (10). The cross sectional area of the abdominal shunt path was assumed to be 20 percent of the area of the current path through the chest.

Figure 8 shows a plot of the relative voltage step-up recorded between spot electrodes 2 and 3 vs. ejection fraction for a family of simulations with ejection fractions ranging from zero to 95 percent. In this computational experiment stroke volume was increased stepwise by reducing the radii of intracavitary blood and adjusting cardiac muscle radii accordingly. Data points represent maximal change in electrical potential recorded on the anterior chest of 3D finite element models. The smooth curve represents the corresponding analytical model of Expressions (10), in which the area of the abdominal current shunt was estimated from radiograph-like images of Figure 6 to be 1/5th the cross section of the front-to-back current path through lung and heart tissue above the diaphragm.
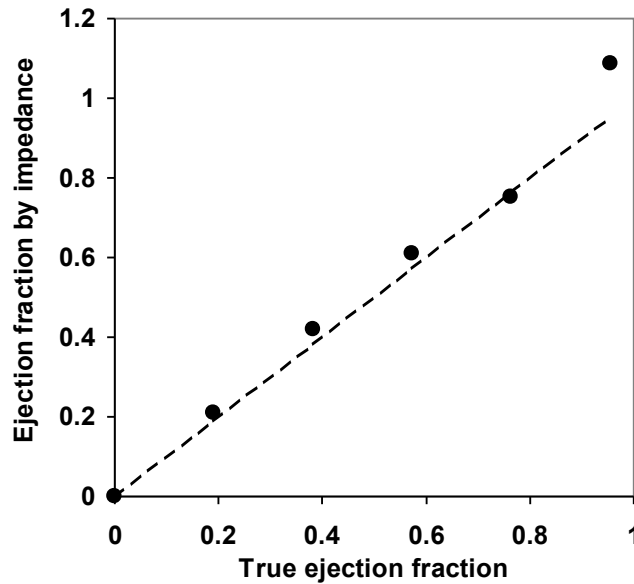
Figure 9. Ejection fraction calculated from chest impedance changes using an analytical model, plotted against actual ejection fraction in a corresponding three dimensional finite element model. Dashed line represents the line of identity.

Figure 9 shows an alternative rendition of these results in which ejection fraction was back calculated from the impedance by solving the quadratic equation (11), compared to actual stroke volume in the 3D model. In these thought experiments the value for blood resistivity was the exact given value, as were the fractions of blood, cardiac muscle, and lung in Column 1. These data do not include the effects of breathing, and so describe heartbeats that occur between breaths.

For comparison Figure 10 illustrates results for finite element models at end inspiration after a normal quiet breath and after a deep breath. In the inspiratory models for a shallow and for a deep breath, the anterior-posterior dimension of the chest was increased by either 0.5 cm or 1 cm, the right-left dimension of the chest was increased by either 1 cm or 2 cm, and the diaphragm was moved toward the feet either 2 cm or 5 cm. The distance between the center of the heart and the diaphragm was increased in proportion to the overall vertical expansion of the chest, as if the entire mediastinum were a simple elastic material, stretched in the head to foot dimension. In addition the resistivity of lung was increased by a factor equal to the fractional increase in lung volume, either $(7.0 + 0.5)/7.0 = 1.07$, or $(7.0 + 1.0)/7.0 = 1.14$, to reflect inflation of the lungs with air and assuming a resting total lung volume of 7 liters and tidal volumes of 500 ml (quiet breath) or 1000 ml (deep breath) in a normal adult human. The effect of breathing on the relative impedance step-up is indicated in Figure 10.
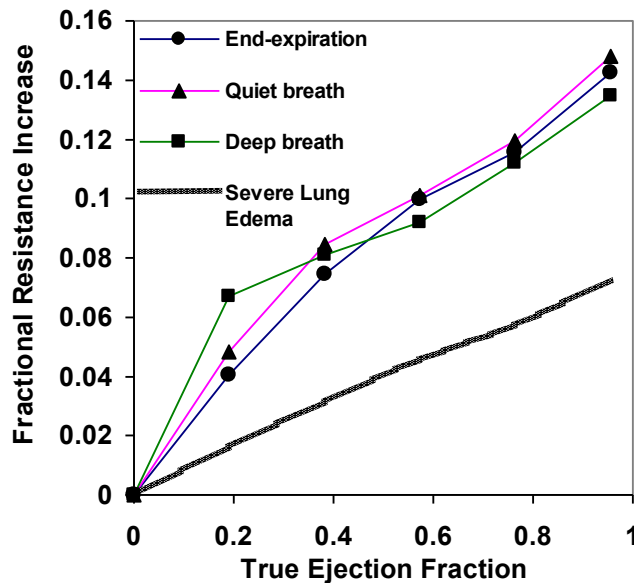
Figure 10. Ejection fraction calculated from chest impedance changes in three-dimensional models of the human torso with zero, shallow, and deep inspiration, accompanied by expansion of the chest and movement of the diaphragm and of the heart. Effects of pulmonary edema with lung impedance reduced from 1500 ohm-cm to 500 ohm-cm are also shown.

The results show little disruption of the cardiogenic impedance signal with either quiet or deep breathing in these models.

The stippled line in Figure 10 represents a simulation of severe pulmonary edema in which lung resistivity was reduced from 1500 ohm-cm to 500 ohm-cm, nearly that of muscle tissue. In this case there is about a 50 percent reduction in the cardiogenic impedance signal, compared to the normal state.

The thought experiments and computer simulations presented here demonstrate a preliminary proof of concept that precordial front-to-back electrodes can be used in conjunction with a constant current, tetrapolar impedance recording system and an appropriate analytical model to provide an meaningful estimates of ventricular ejection fraction. In the presence of pulmonary edema, estimates of stroke volume are reduced by about half.

Discussion

Monitoring of cardiac ejection fraction non-invasively and painlessly on a beat-by beat basis may be possible in a way that can be explained and understood in terms of basic anatomy, physiology, and physics. There is much virtue in measuring left ventricular ejection fraction continuously in critically ill patients such as those at risk of circulatory shock[5]. Ejection fraction is a direct measure of heart performance that changes from moment to moment. If end diastolic volume can also be estimated, for sample using something as simple as biplane chest radiographs and an ellipsoidal model, then absolute stroke volume and cardiac output can be computed. If arterial and central venous blood pressures are also monitored intermittently or continuously then peripheral vascular resistance (total peripheral resistance, or TPR) can be known. Anesthetic overdose, for example, decreases TPR and shock increases TPR if autonomic reflexes are intact. Hence the ability to assess TPR noninvasively with minimal risk provides a substantial aid to clinicians attempting to build a mental model of the cardiovascular system for a particular patient in settings such as the operating room, the critical care unit, or the emergency department. Combining noninvasive flow-related data from impedance cardiography with non-invasive arterial blood oxygen saturation by pulse oximetry could be especially useful for assessing the overall efficacy of the circulation. The performance of critical care physicians and anesthesiologists could be boosted by moment to moment knowledge of peripheral perfusion, obtained at little marginal cost and essentially zero risk to the patient. In some cases Swan-Ganz catheter placement for measurement of cardiac output by thermal dilution could be avoided, reducing the cost and risk of complications.

Acceptance of conventional impedance cardiography has been limited in the past for several reasons, including variable accuracy among disease states, poor precision, and uncertain biological meaning[16]. Validation studies show a general over-estimation of cardiac output determined by conventional methods and formulas[4, 5]. However, the technique gives falsely low values especially in patients with congestive heart failure and dilated, hypo-dynamic hearts[12]. The literature is further muddied by alternative modes of display of the impedance cardiogram, including absolute impedance change, ΔZ, vs. its derivative, dZ/dt, and even alternate polarities, ΔZ vs. $-\Delta Z$. Since all accepted techniques for measuring blood flow in patients have known errors, a true "gold standard" does not exist[5], and doubts persist about the accuracy of any new method. (This state of affairs argues for the value of finite element modeling as a validation tool, in which actual stroke volume can be known exactly.)

Most importantly, the anatomic and physiologic mechanisms that generate the observed changes in axial, whole-chest impedance with each heartbeat have remained unclear[9, 12, 13, 15]. Detailed studies by this author (results not shown) and by Wang and Patterson[9] have revealed a complex mosaic of increases and decreases in impedance of the heart, great vessels, and lungs. The impedance increase caused by the blood volume reduction in the heart is largely cancelled by the impedance decreases caused by expansion of the great vessels and cardiac atria with blood. In this situation, where quantities close

together in value are subtracted, a small percentage change in one component can produce a large percentage change in the net result. The resulting mosaic of hard-to-separate factors and may not provide a reliable basis for the calculation of stroke volume.

The inadequacy of the original Kubicek formula for stroke volume, based on the time derivative of impedance changes of the whole chest in the head-to-foot direction, has been suggested recently by Faes and coworkers[17], who studied the joint causes of impedance change due to blood entering the aorta from the heart, as well as blood leaving the aorta due to arterial runoff. They found the outflow problem was not solved by the classical Kubicek formula based on neck-to-abdomen impedance, and they confirmed their results experimentally. Another skeptical review, subtitled "more questions than answers", was presented by Wang and coworkers[8], who found poor correlation between current generation impedance cardiography devices and invasive measurements of cardiac output, especially in heart failure patients, and suggested the need for further research regarding accuracy.

By changing the axis, placement, and shape of electrodes for impedance cardiography to isolate the contribution of the cardiac ventricles to the impedance signal, one can increase the signal level and signal-to-noise ratio roughly 30 times. The measured impedance change is related not to the absolute stroke volume, but rather to the ejection fraction (stroke volume divided by end-diastolic volume). This insight explains the reduced signals in congestive heart failure (when ejection fraction is expected to be abnormally low).

This insight is, as one might expect, not entirely new. Bonjer and coworkers in 1952 studied a variety of alternative electrode placements for detecting the cardiogenic impedance signal in anesthetized dogs in an attempt to understand the mechanism of their origin[15]. As have others before and since, they found small signals, paradoxes, and contradictions of predictions based on an idealized cylindrical conductor. "On the other hand", they reported, "remarkable differences were seen when one electrode was placed on the sternum and the other on the vertebral column. The interpretation of the resulting curves however was found to be very difficult." Now, over half a century later, we can confirm this original observation and offer a model appropriate for its rational interpretation.

A major artifact in impedance cardiographic records comes from chest impedance changes with breathing. Although breathing does cause large changes in chest impedance, especially when measured from side to side[4], the impedance cardiogram can always be sampled between breaths. Further, the results of Figure 10 suggest that the difference in chest impedance accompanying ventricular ejection is not especially sensitive breathing when front-to-back electrodes are employed.

A second major artifact in impedance cardiography relates to excess fluid in the lungs. Pulmonary edema can reduce baseline pulmonary resistivity ρ_L and also composite resistivity ρ_1 of the front-to-back column including the heart. In congestive heart failure, however, the proportion of tissue volume in this column occupied by blood, σ_b, will

increase somewhat with dilation of the ventricles (roughly in proportion to the increase in heart diameter, since Column 1 by definition includes the heart cross section). The net effects of congestive heart failure with pulmonary edema upon the relative increase in chest impedance per unit of ejection fraction $\frac{\rho_L - \rho_b}{\rho_1(0)}\sigma_b$ are partially offsetting. As shown in Figure 10, severe pulmonary edema only can reduce the impedance signal by about half. Once understood, the effect of pulmonary edema is not mysterious or a cause for abandonment of the technique. Pulmonary edema is easily recognized clinically and an astute clinician can make an appropriate mental correction. A major reason for reduced impedance change with heart failure using the AP impedance axis is true reduction in ejection fraction, characteristic of heart failure itself.

A third artifact in impedance cardiography relates to changes in the resistance of flowing blood in tubes, caused by the axial accumulation and the orientation of erythrocytes[18]. The longitudinal resistance of blood decreases slightly (up to -20%) with flow, contributing to the net decrease in chest impedance during cardiac systole with conventional head-to-foot electrode placement. Interestingly, however, transverse resistance increases with flow to a lesser degree (roughly half as much, up to +10%). Hence the effect is different with front-to-back electrode placement and muted by the relatively lesser volume fraction of the thoracic aorta in the current field.

Prior methods of calculating stroke volume from the chest impedance signal were based upon incomplete understanding of the source of thoracic impedance changes during the cardiac cycle. The weakness of the technique was not in the technology for impedance measurement but in the way the technology was employed and the way the signal was interpreted. In principle anterior-posterior impedance cardiography as described here can be implemented with electronics that have been tested and used clinically for decades. The new impedance axis presented here can boost signal strength, reduce noise, demystify the impedance cardiogram, and allow clinicians to interpret chest impedance changes with greater confidence. Although true stroke volume remains hard to measure, ejection fraction is not. The proposed approach represents a partial solution of a classical open problem in biomedical engineering: how to measure cardiac function noninvasively and accurately on a beat-by-beat basis. Incompletely understood for decades, impedance cardiography deserves new respect.

Appendix 1: reduced lung resistivity during right ventricular ejection

A composite conductivity model accommodates varying proportions in the lungs of blood (subscript b), non-blood tissue (subscript t), and gas (subscript g). For resistivities, ρ, and conductivities $1/\rho$, and volume fractions of lung components, σ, the composite conductivity is

$$\frac{1}{\rho_L} = \frac{\sigma_b}{\rho_b} + \frac{\sigma_t}{\rho_t} + \sigma_g \cdot 0$$

The volume fraction of blood in the lungs changes as blood is ejected into the pulmonary arteries and drains gradually from the pulmonary veins. The blood volume change in the lungs is approximately the product of net ejection fraction, x, and the right ventricular end diastolic volume, $V_{RV}(0)$. For lung volume V_L, we can write

$$\frac{1}{\rho_.(x)} = \frac{1}{\rho_L(0)} + \frac{V_{RV}(0)}{\rho_b V_L} x = \frac{1}{\rho_L(0)}\left(1 + \frac{\rho_L(0)}{\rho_b} \cdot \frac{V_{RV}(0)}{V_L} x\right) = \frac{1}{\rho_L(0)}(1 + \beta_L x),$$

for combined correction constant β_L. So for time-varying lung resistivity we have, using when needed the approximation for small values $\varepsilon \ll 1$ $1/(1+\varepsilon) \approx 1 - \varepsilon$,

$$\rho_{lu}(x) = \frac{\rho_L(0)}{1 + \beta_L x} \approx \rho_L(0)(1 - \beta_L x),$$

where

$$\beta_L = \frac{\rho_L(0)}{\rho_b} \frac{V_{RV}(0)}{V_L} .$$

For example, with lung resistivity = 1500 ohm-cm, blood resistivity = 150 ohm-cm, right end diastolic ventricular volume = 100 ml, and lung volume = 7000 ml, we would have $\beta_L = 0.14$. For an ejection fraction of 50 percent there is about a 7 percent decrease in lung resistivity.

Appendix 2: iterative solution of the finite element model

Body tissues are modeled as a matrix of nodes representing rectangular solid control volumes dx·dy·dz in a 6-way mesh. It is helpful to represent the 6 neighbors of a particular indexed node by directions N, S, E, W, F, B, named for north, south, east, west, front, and back. Each node is located at the center of its control volume, and the nodes are spaced distances dx, dy, and dz apart.

We wish to solve Kirchoff's current law for each node in the system to find the steady-state electrical field throughout the volume of the model for the resistive case. Let the resistivity for an indexed node be defined as ρ, and let the resistivities for the six neighboring nodes be defined as ρ_E, ρ_W, etc. Similarly, let the electrical potential at the indexed node be defined as U, and let the potentials of its neighboring nodes be defined as U_E, U_W, etc. Then, the directional resistances (resistivity times path length divided by area) representing the six pathways to and from each interior node are

$$R_E = \frac{(\rho + \rho_E)}{2}\frac{dx}{dy \cdot dz} \; , \; R_W = \frac{(\rho + \rho_W)}{2}\frac{dx}{dy \cdot dz} \; , \; R_N = \frac{(\rho + \rho_N)}{2}\frac{dy}{dx \cdot dz} \; , \; \text{etc.}$$

By Kirchoff's current law the sum of currents into and out of the node using Ohm's law must be zero. So,

$$\frac{U_E - U}{R_E} + \frac{U_W - U}{R_W} + \frac{U_N - U}{R_N} + \frac{U_S - U}{R_S} + \frac{U_F - U}{R_F} + \frac{U_B - U}{R_B} = 0$$

or

$$U\left\{\frac{1}{R_E} + \frac{1}{R_W} + \frac{1}{R_N} + \frac{1}{R_S} + \frac{1}{R_F} + \frac{1}{R_B}\right\} = \frac{U_E}{R_E} + \frac{U_W}{R_W} + \frac{U_N}{R_N} + \frac{U_S}{R_S} + \frac{U_F}{R_F} + \frac{U_B}{R_B} .$$

In terms of pathway conductivities, $\mu = 1/\rho$, we must have

$$U = \frac{\mu_E U_E + \mu_W U_W + \mu_N U_N + \mu_S U_S + \mu_F U_F + \mu_B U_B}{\mu_E + \mu_W + \mu_N + \mu_S + \mu_F + \mu_B} \; ,$$

for Kirchoff's current law to be satisfied. The electrical potential at any interior node is a weighted average of the surrounding potentials with weights determined by the local conductivities.

Solving this expression recursively allows for iterative solution of the entire system, given the initial conditions, including fixed electrode potentials at the boundaries. If superscript, n, represents the n-th step of iteration, then beginning at step n = 0 with seed

values of given potentials at the electrodes and an initial guess of the average electrode potential at other nodes, one can evaluate recursively the expression

$$U^{n+1} = \frac{\mu_E U_E^n + \mu_W U_W^n + \mu_N U_N^n + \mu_S U_S^n + \mu_F U_F^n + \mu_B U_B^n}{\mu_E + \mu_W + \mu_N + \mu_S + \mu_F + \mu_B} \,.$$

for each node in the model. The recursion is stopped when the root mean square difference between iterations for all N nodes in the model, $\sqrt{\dfrac{1}{N}\sum_N \left(U^{n+1} - U^n\right)^2}$, becomes less than a small prescribed value. To speed convergence an acceleration factor, $\alpha < 1$, can be introduced and the iterates upgraded using the expression

$$U^{n+1} \leftarrow U^{n+1} + \alpha\left(U^{n+1} - U^n\right).$$

The forgoing numerical method was implemented in Visual Basic code within an Excel spreadsheet on ordinary personal computers operating under Microsoft Windows. The computer code was validated by comparison with simple test cases, including uniform resistivity rectangular solids and parallel uniform resistivity columns, for which analytical solutions are available. Using $\alpha = 0.95$, rapid convergence in fewer than 300 iterations was obtained for all cases tested.

References

1. Nyboer J, Bango S, Barnett A, Halsey RH. Radiocardiograms: Electrical impedance changes of the heart in relation to electrocardiograms and heart sounds. Journal of Clinical Investigation 1940; 19:773 (abstract).
2. Tsadok S. The historical evolution of bioimpedance. AACN Clin Issues 1999; 10:371-84.
3. Kubicek WG, Witsoe DA, Patterson RP, Mosharrafa MA, Karnegis JN, From AHL. DEVELOPMENT AND EVALUATION OF AN IMPEDANCE CARDIOGRAPHIC SYSTEM TO MEASURE CARDIAC OUTPUT. Houston, Texas: National Aeronautics and Space Administration, Manned Spacecraft Center, 1967.
4. Geddes LA, Baker LE. Principles of Applied Biomedical Instrumentation, Second edition. John Wiley & Sons, New York, 1975.
5. Van De Water JM, Miller TW, Vogel RL, Mount BE, Dalton ML. Impedance cardiography: the next vital sign technology? Chest 2003; 123:2028-33.
6. Packer M, Abraham WT, Mehra MR, et al. Utility of impedance cardiography for the identification of short-term risk of clinical decompensation in stable patients with chronic heart failure. J Am Coll Cardiol 2006; 47:2245-52.
7. Raaijmakers E, Faes TJ, Goovaerts HG, Meijer JH, de Vries PM, Heethaar RM. Thoracic geometry and its relation to electrical current distribution: consequences for electrode placement in electrical impedance cardiography. Med Biol Eng Comput 1998; 36:592-7.

8.   Wang DJ, Gottlieb SS. Impedance cardiography: more questions than answers. Curr Cardiol Rep 2006; 8:180-6.

9.   Wang L, Patterson R. Multiple sources of the impedance cardiogram based on 3-D finite difference human thorax models. IEEE Trans Biomed Eng 1995; 42:141-8.

10.   Patterson R, Wang L, McVeigh G, Burns R, Cohn J. Impedance cardiography: the failure of sternal electrodes to predict changes in stroke volume. Biol Psychol 1993; 36:33-41.

11.   Van de Water JM, Mount BE, Barela JR, Schuster R, Leacock FS. Monitoring the chest with impedance. Chest 1973; 64:597-603.

12.   Patterson RP, Wang L, Raza SB. Impedance cardiography using band and regional electrodes in supine, sitting, and during exercise. IEEE Trans Biomed Eng 1991; 38:393-400.

13.   Critchley LA, Peng ZY, Fok BS, James AE. The effect of peripheral resistance on impedance cardiography measurements in the anesthetized dog. Anesth Analg 2005; 100:1708-12.

14.   Miclavcic D, Pavselj N, Heart FX. Electrical properties of tissues. In: Akay M, ed. Wiley Encyclopedia of Biomedical Engineering. Vol. 6. New York: John Wiley & Sons, 2006:3578-3589.

15.   Bonjer FH, Van Den Berg J, Dirken MN. The origin of the variations of body impedance occurring during the cardiac cycle. Circulation 1952; 6:415-20.

16.   Kosicki J, Chen LH, Hobbie R, Patterson R, Ackerman E. Contributions to the impedance cardiogram waveform. Ann Biomed Eng 1986; 14:67-80.

17.   Raaijmakers E, Faes TJ, Goovaerts HG, de Vries PM, Heethaar RM. The inaccuracy of Kubicek's one-cylinder model in thoracic impedance cardiography. IEEE Trans Biomed Eng 1997; 44:70-6.

18.   Sakamoto K, Kanai H. Electrical characteristics of flowing blood. IEEE Trans Biomed Eng 1979; 26:686-95.